Optimal protocol for spin-orbit torque switching of a perpendicular nanomagnet

Sergei M. Vlasov,[1,*] Grzegorz J. Kwiatkowski,[2,*] Igor S. Lobanov,[1] Valery M. Uzdin,[1] and Pavel F. Bessarab[1,2,3,†]

[1] *ITMO University, 197101 St. Petersburg, Russia*
[2] *Science Institute of the University of Iceland, 107 Reykjavík, Iceland*
[3] *School of Science and Technology, Örebro University, Fakultetsgatan 1, SE-70281 Örebro, Sweden*

It is demonstrated by means of the optimal control theory that the energy cost of the spin-orbit torque induced reversal of a nanomagnet with perpendicular anisotropy can be strongly reduced by proper shaping of both in-plane components of the current pulse. The time dependence of the optimal switching pulse that minimizes the energy cost associated with joule heating is derived analytically in terms of the required reversal time and material properties. The optimal reversal time providing a tradeoff between the switching speed and energy efficiency is obtained. A sweet-spot balance between the fieldlike and dampinglike components of the spin-orbit torque is discovered; it permits for a particularly efficient switching by a down-chirped rotating current pulse whose duration does not need to be adjusted precisely.

I. INTRODUCTION

The discovery of spin-orbit torque (SOT) is a notable milestone in the development of spintronics as it has made it possible to boost the efficiency of electrical manipulation of magnetism compared to conventional spin transfer torques [1–3]. Magnetization switching by current-induced fieldlike (FL) and dampinglike (DL) components of SOT is a particularly important application providing a basis for low-power bit operations in nonvolatile technologies [4, 5].

Typically, a SOT-induced magnetization reversal is realized by applying an in-plane current in a heavy-metal (HM) layer on which a switchable ferromagnetic (FM) element is placed. Elements with perpendicular magnetic anisotropy (PMA) are under a special focus due to their technological relevance. In a conventional protocol involving a one-dimensional direct current, the deterministic reversal of the PMA element relies only on the DL SOT [6, 7]. As a result, the switching current density and thereby the energy cost of switching are not as low as they could possibly be if the FL SOT was also used [8]. FL SOT-induced switching can also be realized, but this requires a precise control over the current pulse duration so as to avoid back-switching [9]. Moreover, to achieve definite switching of the PMA element, some symmetry breaking needs to be established either by applying an external magnetic field [2, 3, 10], which can be mimicked by exchange coupling with an additional magnetic layer [11–14], or by introducing lateral asymmetry [15, 16] or tilted anisotropy [17, 18]. Out-of-plane torque for field-free switching can also be generated due to the low-symmetry point groups at the HM/FM interfaces [19] or thanks to the out-of-plane polarization of spin currents generated in an additional magnetic layer [20].

Note that the complications associated with the conventional SOT-induced magnetization reversal originate from use of one-dimensional direct current. Such a simple switching pulse provides a limited control over switching and makes it hard to realize the full potential of SOT.

The issues arising in SOT-induced switching can be solved by proper shaping of the current pulse. Pulse optimization has been studied extensively in the past in the context of magnetization reversal by means of applied magnetic field [21–29] and spin-transfer torque [30, 31]. For SOT-induced reversals, this approach remains unexplored, although its potential has recently been demonstrated by Zhang *et al.* [32] who proposed to use both in-plane components of the current to realize field-free switching of a PMA element; assuming a fixed magnitude but variable direction of the current, they obtained a strong reduction in the switching current density and derived a pulse yielding the shortest switching time. However, constraints imposed on the current pulse prevented previous studies from identifying the theoretical minimum of the energy cost of SOT-induced switching. Optimization of the switching protocols with respect to materials properties and identification of the right balance between switching speed and energy efficiency have also been missing so far despite the great fundamental and technological importance of this analysis. Moreover, it is still unclear whether the protocols involving 2D currents are stable enough against thermal fluctuations to be realized in practice.

In this article, we identify energy-efficient switching pulses by applying a systematic approach based on the optimal control theory. To make the most of the pulse optimization, we do not apply any constraints on the pulse shape and consider independent variations of both in-plane components of the current. We obtain a complete analytical solution for optimal control paths (OCPs) of field-free magnetization switching, i.e. the reversal trajectories minimizing the energy cost associated with joule heating, and derive optimal switching pulses from the obtained OCPs.

Our analytical solution provides a theoretical limit for energy-efficient control of SOT-induced magnetization switching and reveals noteworthy exact results connecting the minimum energy cost, optimal switching current and switching time with relevant materials properties. We uncover a previously overlooked sweet-spot ratio of the FL and DL torques for which a particularly appealing switching protocol is possible. It is robust, corresponds

to the lowest energy cost and shortest switching time, and involves a quite simple switching pulse that can likely be realized in the laboratory.

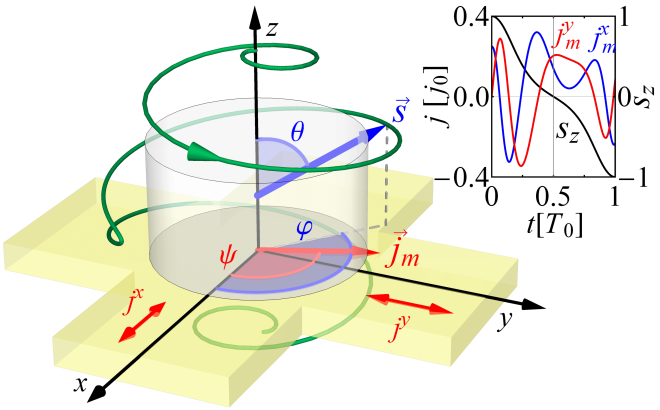

Figure 1. Energy-efficient switching of a PMA nanoelement (cylinder) by an optimal 2D electric current pulse $\vec{j}_m$ flowing in the heavy-metal substrate (cross). The calculated optimal control path for the switching for $\alpha = 0.1$ and $\xi_D = 3.56\xi_F$ is shown with the green line. The direction of the normalized magnetic moment $\vec{s}$ of the element (optimal current $\vec{j}_m$) is shown with the blue (red) arrow. The inset shows the time dependence of x and y components of $\vec{j}_m$ and z component of $\vec{s}$.

II. MODEL

Figure 1 shows the simulated PMA element whose magnetic moment is reversed by an in-plane current via SOT. The element is assumed small enough to be treated essentially as a single-domain particle at any time of the reversal process. The energy E of the system is defined by the anisotropy along the z axis,

$$E = -Ks_z^2, \tag{1}$$

where s_z is a z component of the normalized magnetic moment $\vec{s}$ and $K > 0$ is the anisotropy constant. The task is to identify the optimal current pulse that reverses the magnetic moment from $s_z = 1$ at $t = 0$ to $s_z = -1$ at $t = T$, with T being the switching time. Both the amplitude and the direction of the current $\vec{j}$ in the heavy-metal layer are allowed to vary in time. This can be realized in the cross-type geometry permitting independent control of both in-plane components of the current; see Fig. 1. The efficiency of the reversal is naturally defined by the amount of joule heating generated in the resistive circuit during the switching process [31]. In particular, the optimal reversal is achieved when the cost functional

$$\Phi = \int_0^T |\vec{j}|^2 dt, \tag{2}$$

is minimized. This optimal control problem is subject to a constraint imposed by the zero-temperature Landau-Lifshitz-Gilbert (LLG) equation describing the dynamics of the magnetic moment under SOT [33]:

$$\begin{aligned}\dot{\vec{s}} = &-\gamma\vec{s}\times\vec{b} + \alpha\vec{s}\times\dot{\vec{s}} \\ &+ \gamma\xi_F\vec{s}\times(\vec{j}\times\vec{e}_z) + \gamma\xi_D\vec{s}\times\left[\vec{s}\times(\vec{j}\times\vec{e}_z)\right].\end{aligned} \tag{3}$$

Here, γ is the gyromagnetic ratio, α is the damping parameter, $\vec{e}_z$ is the unit vector along the z axis, and $\vec{b}$ is the anisotropy field: $\vec{b} \equiv -\mu^{-1}\partial E/\partial\vec{s}$, with μ being the magnitude of the magnetic moment. The third and the fourth terms on the rhs of Eq. (3) represent FL and DL components of the SOT, respectively. The coefficients ξ_F and ξ_D are defined by the spin Hall angle, saturation magnetization, and thickness of the FM element, as well as by dimensionless factors – efficiencies – characterizing the weights of the SOT components [34].

III. RESULTS

To find the optimal switching current $\vec{j}_m(t)$ that makes Φ minimum, we follow the paradigm we applied earlier to the magnetization reversal induced by applied magnetic field [35]: the energy cost is first expressed in terms of the switching trajectory and then minimized so as to find the OCPs for the switching process; after that, the optimal switching pulse $\vec{j}_m(t)$ is derived from the OCPs. Qualitative difference between the field torque and SOT makes these calculations significantly more involved compared to Ref. [35]. Here, we only sketch briefly the derivations, but a complete analytical solution to this nonlinear problem is available at [36].

1. *Optimal control path for magnetization switching*

We start by expressing the amplitude of $\vec{j}$ in terms of the dynamical trajectory using Eq. (3):

$$j = \frac{2K}{\mu}\frac{(1+\alpha^2)\tau_0\dot{\theta} + \alpha\sin\theta\cos\theta}{(\alpha\xi_\mathrm{D} - \xi_\mathrm{F})\cos\varphi' - (\alpha\xi_\mathrm{F} + \xi_\mathrm{D})\cos\theta\sin\varphi'}. \tag{4}$$

Here, $\tau_0 = \mu(2K\gamma)^{-1}$ defines the timescale of Larmor precession, θ and φ are the polar and azimuthal angles of $\vec{s}$, respectively, and $\varphi' \equiv \varphi - \psi$, with ψ being the angular coordinate of the current (see Fig. 1). It is clear from Eq. (4) that for a given magnitude of the current-generated torque, overall increase in the SOT coupling coefficients leads to a proportional decrease in the switching current, and thereby the energy cost. To elucidate a nontrivial effect of the SOT parameters, we introduce a variable β characterizing the balance between the SOT components, via the following parametrization:

$$\xi_\mathrm{F} = \xi\cos\beta, \quad \xi_\mathrm{D} = \xi\sin\beta, \tag{5}$$

where ξ is the magnitude of the total SOT coupling, i.e. $\xi \equiv \sqrt{\xi_\mathrm{D}^2 + \xi_\mathrm{F}^2}$.

On substituting Eq. (4) into Eq. (2), the energy cost of the reversal becomes a functional of the switching trajectory. Taking into account Eq. (5) and minimizing Φ with respect to φ', we obtain an optimal value of φ with respect to ψ (see also Ref. [32]):

$$\varphi' = \varphi - \psi = \arctan\left[\tan(\beta+\eta)\cos\theta\right], \tag{6}$$

where $\eta \equiv \arctan(\alpha)$. After eliminating the φ' dependence of Φ with the use of Eq. (6), the Euler-Lagrange equation for θ can be derived [36]. Its solution satisfying the boundary conditions $\theta(0) = 0$, $\theta(T) = \pi$ is expressed in terms of Jacobi elliptic functions [36] (see Appendix A for the definition of the elliptic integrals and functions). Finally, optimal $\varphi(t)$ is obtained from optimal $\theta(t)$ using the equation of motion [see Eq. (3)], where ψ is eliminated using Eq. (6). In this way, the OCP describing the switching trajectory that minimizes the energy cost is completely defined. It corresponds to the magnetic moment rotating steadily from the initial state minimum to the final one and at the same time precessing around the anisotropy axis. Depending on whether the sign of $\tan(\beta+\eta)$ is negative or positive, the sense of precession changes before or after the system crosses the energy barrier, respectively. However, the barrier crossing happens exactly at $t = T/2$, which results from a general symmetry of the solution $\theta_m(t)$: $\theta_m(T/2+t') = \pi - \theta_m(T/2-t')$, $0 \le t' \le T/2$. The OCP for $\alpha = 0.1$, $\xi_D = 3.56\xi_F$, and $T = T_0$ [see Eq. (12)] is shown in Fig. 1.

2. *Optimal switching pulse*

Optimal control $\vec{j}_m(t)$ can be derived from the OCP using Eqs. (4) and (6). It corresponds to a rotating current whose sense of rotation changes together with that of the magnetic moment precession around the anisotropy axis. Although the form of $\vec{j}_m(t)$ is rather complex in a general case (see the inset in Fig. 1), the following properties hold exactly. For finite damping, the amplitude of the optimal current is modulated such that it reaches a maximum value exactly at $t = T/4$ and a minimum value at $t = 3T/4$, with the difference between the extremal values given by

$$\Delta j_\mathrm{m} = \frac{4\alpha j_0}{\sqrt{1+\alpha^2}\left(|\cos(\beta+\eta)|+1\right)}, \tag{7}$$

where $j_0 = K(\mu\xi)^{-1}$. Equation (7) particularly signifies that the current amplitude is constant for zero damping. The average current amplitude can also be expressed analytically:

$$\langle j_\mathrm{m}\rangle = \frac{4j_0\tau_0\sqrt{1+\alpha^2}\mathcal{K}\left[\sin^2(\beta+\eta)\right]}{T}, \tag{8}$$

where $\mathcal{K}[.]$ is the complete elliptic integral of the first kind (see Appendix A). Notably, the average current does not depend on the height of the energy barrier defined by the magnetic anisotropy. Additionally, the following symmetry holds in general: $j_\mathrm{m}(0) = j_\mathrm{m}(T/2) = j_\mathrm{m}(T)$.

3. *Minimum energy cost of magnetization switching*

The minimum energy cost Φ_m is a monotonically decreasing function of the switching time exhibiting two asymptotic regimes (see Fig. 2). For fast switching, $\Phi_\mathrm{m}(T)$ scales inversely with T and does not depend on the magnetic potential:

$$\Phi_\mathrm{m} \approx \frac{4(1+\alpha^2)\mathcal{K}^2\left(\sin^2(\beta+\eta)\right)}{T\gamma^2\xi^2}, \quad T \ll (\alpha+1/\alpha)\tau_0. \tag{9}$$

At infinitely long switching time, Φ_m approaches the lower limit:

$$\Phi_\mathrm{m} \to \frac{4\alpha K\log\left[1+\tan^2(\beta+\eta)\right]}{\mu\gamma\xi^2\sin^2(\beta+\eta)}, \quad T\to\infty. \tag{10}$$

Intersection of the asymptotics gives a characteristic switching time providing a tradeoff between the switching speed and energy efficiency. For a given T, the energy cost corresponding to the constant-amplitude pulse derived in [32] always exceeds $\Phi_m(T)$ and even diverges at $T \to \infty$ (see Fig. 2).

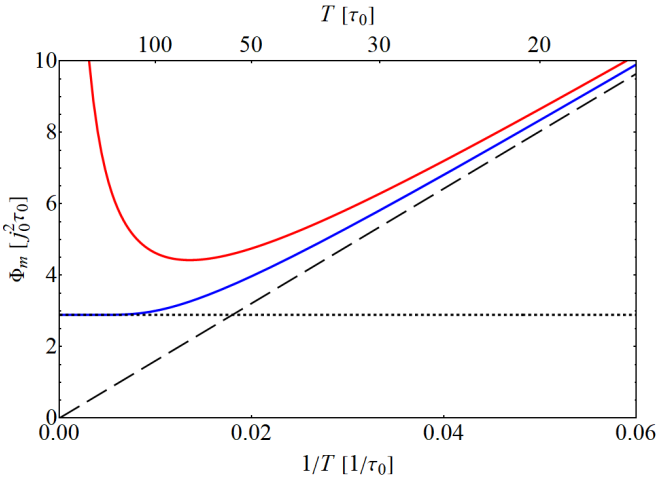

Figure 2. Minimum energy cost of magnetization switching (blue line) as a function of the inverse of the switching time for $\alpha = 0.1$ and $\xi_D = 3.56\xi_F$. Red line shows the energy cost corresponding to the constant-amplitude pulse derived in [32] for the same set of parameters. Dashed and dotted lines show short and infinite switching time asymptotics, respectively.

Φ_m as a function of β is shown in Fig. 3. Φ_m diverges when $\alpha\xi_\mathrm{D} = \xi_\mathrm{F}$ signifying no switching for this ratio of the SOT coefficients, which was also pointed out in Ref. [32]. The divergence originates from the vanishing torque in the direction of increasing θ at the equator. To

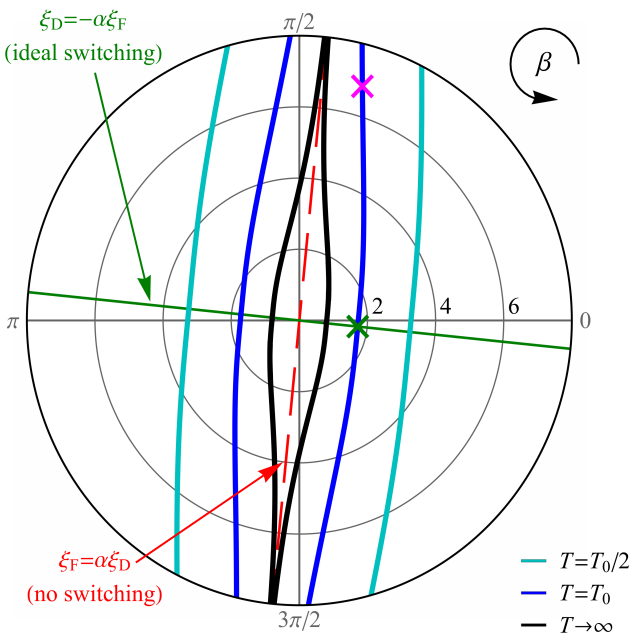

Figure 3. Minimum energy cost of magnetization switching in units of $j_0^2\tau_0$ as a function of β for $\alpha = 0.1$ and several values of the switching time. Green solid line indicates the ideal ratio of the SOT coefficients; red dashed line marks the ratio that prohibits switching. The green (magenta) cross indicates ideal (nonideal) parameter values for which the optimal current pulse is shown in Fig. 4(a) (inset of Fig. 1).

realize switching in this case, an additional force such as external magnetic field needs to be applied to the system, similar to what is done in conventional SOT-induced switching [13].

On the other hand, $\Phi_m(\beta)$ has minima at $\beta = \beta^*$, with β^* defined by $\tan(\beta^* + \eta) = 0$. The minima correspond to an ideal ratio between the SOT coefficients,

$$\xi_D = -\alpha\xi_F, \tag{11}$$

for which the switching is particularly efficient. For this ratio, the torque generated by $\vec{j}_m$ is invested entirely into the increase in θ, i.e. only into the motion which is relevant for switching. Such a rational use of an external stimulus can always be achieved for the optimal magnetization reversal induced by applied magnetic field [35] via the adjustment of all three components of the field. For SOT-induced switching, realization of the SOT exclusively in the direction of increasing θ is only possible for the ideal balance between ξ_D and ξ_F due to the confinement of the switching current to xy plane.

The characteristic switching time defined by crossing of the asymptotics of Φ_m [see Eqs. (9) and (10)] also approaches the minimum value (with respect to the variation of β) T_0 for the ideal ratio of the SOT coefficients:

$$T_0 = \frac{(1+\alpha^2)\pi^2}{2\alpha}\tau_0. \tag{12}$$

For $\alpha = 0.1$, T_0 corresponds to just a few oscillations of the magnetic moment. Upon substituting $\beta = \beta^*$ and $T = T_0$ into Eq. (8), the average switching current becomes (here and below, an asterisk signifies a quantity corresponding to the ideal ratio between the SOT coefficients):

$$\langle j_m^* \rangle = \frac{4\alpha j_0}{\pi\sqrt{1+\alpha^2}}. \tag{13}$$

Noteworthy, this characteristic current scales with α in the low damping regime making it significantly smaller than the critical current for conventional SOT-induced switching of a PMA element [6].

4. *Switching protocol for the sweet-spot ratio of the SOT coefficients*

Together with the shortest switching time and improved energy efficiency, the ideal ratio of the SOT coefficients provides particularly simple switching protocol. Indeed, the Euler-Lagrange equation describing the OCP simplifies significantly and becomes identical to that derived for the magnetic field-induced switching [35]. The optimal switching pulse gets simpler as well. Its rotation frequency becomes equal to the resonant frequency of the system:

$$f_m^* \equiv \frac{1}{2\pi}\dot{\psi}_m^* = \frac{\cos(\theta_m^*)}{2\pi\tau_0(1+\alpha^2)}. \tag{14}$$

The frequency decreases monotonically with time and exhibits a symmetry, $f_m^*(T/2 + t') = -f_m^*(T/2 - t')$, $0 \le t' \le T/2$, signifying the sign change exactly at $t = T/2$. Time dependence for the switching current and its frequency for $\alpha = 0.1$, $T = T_0$, and $\xi_D = -\alpha\xi_F$ is shown in Fig. 4. Overall, the switching current for the ideal balance between the SOT coefficients resembles a down-chirped pulse whose rotation reverses at the instant of the barrier crossing and amplitude is fairly constant in the low damping regime [see Eq. (7)].

Motivated by this result, we further investigate whether the substitution of the optimal control by a simplified pulse represented by a rotating current with constant amplitude and time-linear frequency sweep indeed leads to magnetization switching in the PMA element. For this, we simulate the magnetization dynamics induced by current $\vec{j}_s(t)$ given by the following ansatz:

$$\vec{j}_s(t) = j_s\cos\big[\Omega(t)\big]\vec{e}_x + j_s\sin\big[\Omega(t)\big]\vec{e}_y, \tag{15}$$

where $\Omega(t) = 2\pi f_{\max}\left(t - t^2/T\right)$. We additionally include thermal noise in the simulations to verify robustness of the switching (see Appendix B for the details of the magnetization dynamics simulations). We perform the simulations for $T = T_0$, $\alpha = 0.1$, and the ideal ratio of the SOT coefficients. We find that $\vec{j}_s(t)$ reliably induces magnetization switching as long as its amplitude j_s

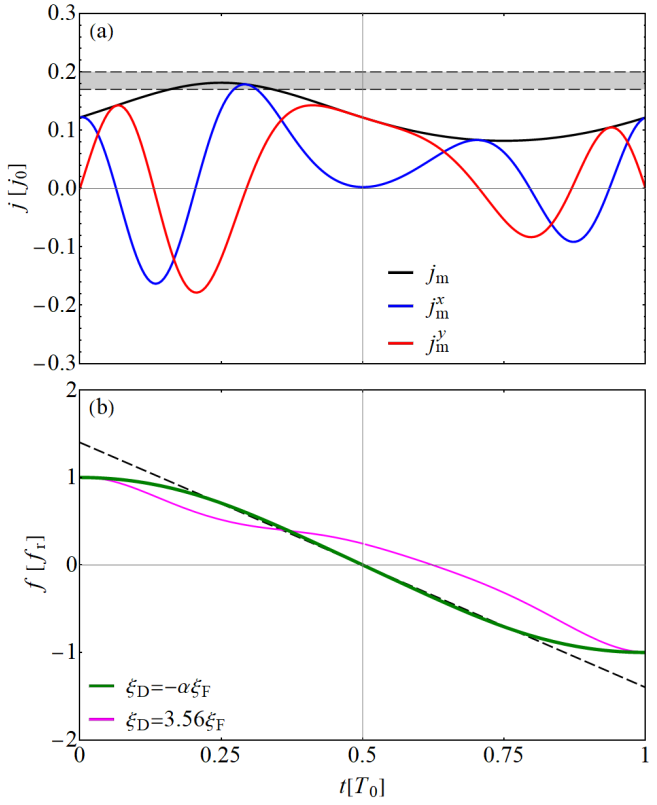

Figure 4. (a) Time dependence of the optimal switching current for the ideal ratio of the SOT coefficients [see Eq. (11)] $\alpha = 0.1$ and $T = T_0$. Gray area in between the dashed lines indicates the range of amplitudes used for the simplified current pulse [see Eq. (15)]. (b) Time dependence of the frequency of the optimal current pulse for the ideal (solid green line) and nonideal (solid magenta line) ratio of the SOT coefficients. Dashed black line shows the frequency variation for the simplified pulse.

is large enough and its initial frequency $f_{\max}$ slightly exceeds the resonant frequency f_r at the energy minimum, $f_r \equiv [2\pi\tau_0(1+\alpha^2)]^{-1}$. In particular, for $f_{\max} = 1.4 f_r$ and a typical for a memory element thermal stability factor [37] of 60 the switching probability increases from 0.89 to 0.97 as j_s changes from $0.17 j_0$ to $0.18 j_0$, and becomes practically unity for $j_s = 0.2 j_0$. As soon as the moment roughly reverses its orientation at $t \approx T$, the pulse can be terminated, but extending the pulse duration beyond T does not compromise switching, as confirmed by our simulations. The absence of unwanted instabilities such as backswitching is expected since interaction of $\vec{j}_s(t)$ with the magnetic moment becomes progressively less effective for $t > T$ where the pulse frequency exceeds the resonant frequency of the system, and the moment stays locked in the reversed position. The switching protocol produced by the rotating current does not require fine-tuning of the pulse duration and is therefore robust.

On the other hand, the simplified switching protocol does require the ratio between the SOT coefficients to be close enough to the ideal value. Otherwise, the optimal switching pulse can be quite different from that described by Eq. (15) [see the inset of Fig. 1 and Fig. 4(b)], and no stable switching on the timescale of moment oscillations can be obtained using the simplified pulse (see Appendix B), although slower reversal involving multiple precession motion can still be achieved regardless of the ratio of the SOT coefficients [38] thanks to the autoresonant excitation [39–41]. It is however expected that slow autoresonant switching is quite sensitive to thermal fluctuations that tend to disturb the phase locking.

IV. CONCLUSIONS AND DISCUSSION

In this work, we have presented a theoretical limit for the minimum energy cost of the SOT-induced magnetization reversal in the PMA nanoelement at zero applied magnetic field and derived the corresponding optimal switching current pulse as a function of the reversal time and relevant material properties. We have identified an ideal ratio of the SOT coefficients corresponding to a particularly efficient, robust, and simple switching protocol. The average switching current for the ideal balance between the DL and FL torques scales with the Gilbert damping parameter, which makes it significantly lower than a critical current in conventional switching protocols. Our results reveal a target for the design of PMA systems for energy-efficient applications and inspire experimental studies of pulse shaping for the optimization of the current-induced magnetization dynamics and switching.

Experimental realization of fast and energy-efficient switching of PMA elements by means of chirped rotating current requires the SOT coefficients to have opposite signs, with FL torque being significantly larger than DL torque [see Eq. (11)]. Several systems where this scenario is realized have been reported; see, e.g., Refs. [42–44] and Table II in [45]. Moreover, the torques can be tuned by inducing piezoelectric strain [46] or generating orbital currents [47].

While only the FL and DL torques are considered here, the SOT can have additional angular dependence [48]. Optimization of the magnetization reversal for such an extended SOT model is a challenging problem that goes beyond the scope of the present study. From general arguments it follows that further decrease in the energy cost is conceivable in the extended model, but this remains to be explored. Nevertheless, some arguments on how the combination of the SOT coefficients in the extended model affects the magnetization switching can be provided without actually solving the optimal control problem; see Appendix C.

ACKNOWLEDGMENTS

The authors would like to thank T. Sigurjónsdóttir and C. Back for helpful discussions. This work was

funded by the Russian Science Foundation (Grant No. 19-72-10138), the Icelandic Research Fund (Grant No. 184949), the University of Iceland Research Fund (Grant No. 15673), and the Swedish Research Council (Grant No. 2020-05110).

Appendix A: Elliptic integrals and functions

The elliptic integral of the first kind is defined as

$$\mathcal{F}(\rho|k) = \int_0^\rho \frac{dr}{\sqrt{1-k\sin^2(r)}}, \tag{A1}$$

where k is the elliptic modulus. The complete elliptic integral of the first kind is given by

$$\mathcal{K}(k) = \mathcal{F}\left(\frac{\pi}{2}\middle|k\right). \tag{A2}$$

The complete elliptic integral of the second kind is defined as

$$\mathcal{E}(k) = \int_0^{\frac{\pi}{2}} \sqrt{1-k\sin^2(r)}\; dr. \tag{A3}$$

The Jacobi amplitude am is defined as an inverse of the elliptic integral of the first kind:

$$u = \mathcal{F}(\rho|k), \tag{A4}$$
$$\rho = \mathrm{am}(u|k). \tag{A5}$$

The Jacobi sn function is defined as

$$\mathrm{sn}(u|k) = \sin(\mathrm{am}(u|k)). \tag{A6}$$

The Jacobi dn function is defined as

$$\mathrm{dn}(u|k) = \sqrt{1-k\,\mathrm{sn}^2(u|k)}. \tag{A7}$$

See Ref. [49] for further information about elliptic functions and integrals.

Appendix B: Magnetization dynamics simulations

Magnetization dynamics simulations were performed in order to verify stable switching of the perpendicular nanomagnet by a rotating current with constant amplitude and time-linear frequency sweep. The simulations were carried out by integrating the LLG equation [see Eq. (3)] equipped with the current pulse $\vec{j}_s(t)$ [see Eq. (15)]. The LLG equation was integrated numerically using the semi-implicit scheme B as described in Ref. [50]. Interaction of the magnetic system with the heat bath was simulated by including a stochastic term in the LLG equation.

Each simulation had three stages: (1) initial equilibration at zero applied current to establish Boltzmann distribution; (2) switching where the current pulse is applied (note that thermal fluctuations were also included during the switching stage); (3) final equilibration at zero applied current. The duration of the switching stage, i.e., the switching time, was chosen to be T_0 [see Eq. (12)]. At the end of the third stage, we inspected the value of s_z (z component of the unit vector $\vec{s}$ in the direction of the magnetic moment); we have taken the value $s_z = -0.5$ as the threshold for the successful switching.

For each value of the amplitude j_s and initial frequency $f_{\max}$ of the current pulse, we repeated simulations $N = 10000$ times in order to accumulate proper statistics. The switching probability is defined as

$$p = N_\mathrm{s}/N, \tag{B1}$$

where N_s is the number of successful reversals.

For the ideal ratio of the SOT components [see Eq. (11)] and any fixed amplitude of the switching current, we find that the largest switching probability is obtained when the frequency sweeping rate roughly coincides with that of the optimal pulse at $t = T/2$ [see Fig. 4(b)]. This situation is achieved when the initial frequency $f_{\max}$ is somewhat larger than the resonant frequency f_r at the energy minimum: $f_{\max} = 1.4 f_r$. We also confirm that extending the current pulse beyond T does not affect the switching probability.

When the ratio of the SOT components deviates from the ideal value, the reversal by the pulse $\vec{j}_s$ becomes progressively less stable. In particular, when the damping-like torque exceeds the fieldlike torque by a factor of 3.56, magnetization switching is realized only for a very narrow range of the parameters j_s, $f_{\max}$.

Appendix C: Extended SOT model

We start with the LLG equation including the extended model for SOT [48]:

$$\begin{aligned}\dot{\vec{s}} = &-\gamma\vec{s}\times\vec{b} + \alpha\vec{s}\times\dot{\vec{s}} + \gamma\vec{s}\times(\vec{j}\times\vec{e}_z)\left[\xi_F + (\vec{e}_z\times\vec{s})^2\xi_2^\perp + (\vec{e}_z\times\vec{s})^4\xi_4^\perp\right] \\ &-\gamma\vec{s}\times(\vec{e}_z\times\vec{s})\left(\vec{s}\cdot\vec{j}\right)\left[\xi_2^\perp + (\vec{e}_z\times\vec{s})^2\xi_4^\perp\right] + \gamma\vec{s}\times\left[\vec{s}\times(\vec{j}\times\vec{e}_z)\right]\xi_D - \gamma\vec{e}_z\times\vec{s}\left(\vec{s}\cdot\vec{j}\right)\left[\xi_2^\parallel + (\vec{e}_z\times\vec{s})^2\xi_4^\parallel\right].\end{aligned} \tag{C1}$$

In this extended model, the current-generated torque is given by the following equation:

$$\begin{aligned}\vec{\mathcal{T}} = \quad & \frac{\gamma}{1+\alpha^2}\vec{s}\times(\vec{j}\times\vec{e}_z)\left(\chi_F+\chi_2^{\perp}\sin^2\theta+\chi_4^{\perp}\sin^4\theta\right)-\frac{\gamma}{1+\alpha^2}\vec{s}\times(\vec{e}_z\times\vec{s})\left(\vec{s}\cdot\vec{j}\right)\left(\chi_2^{\perp}+\chi_4^{\perp}\sin^2\theta\right)\\ & +\frac{\gamma}{1+\alpha^2}\vec{s}\times\left[\vec{s}\times(\vec{j}\times\vec{e}_z)\right]\chi_D-\frac{\gamma}{1+\alpha^2}\vec{e}_z\times\vec{s}\left(\vec{s}\cdot\vec{j}\right)\left(\chi_2^{\parallel}+\chi_4^{\parallel}\sin^2\theta\right),\end{aligned} \tag{C2}$$

where the following notations are introduced:

$$\chi_F=\xi_F-\alpha\xi_D,\ \ \chi_D=\alpha\xi_F+\xi_D,\ \ \chi_2^{\perp}=\xi_2^{\perp}-\alpha\xi_2^{\parallel},\ \ \chi_2^{\parallel}=\alpha\xi_2^{\perp}+\xi_2^{\parallel},\ \ \chi_4^{\perp}=\xi_4^{\perp}-\alpha\xi_4^{\parallel},\ \ \chi_4^{\parallel}=\alpha\xi_4^{\perp}+\xi_4^{\parallel}. \tag{C3}$$

Projections of $\vec{\mathcal{T}}$ on the directions of increasing θ and φ read:

$$\mathcal{T}_\theta=\frac{\gamma j}{1+\alpha^2}\left[\cos(\varphi-\psi)\left(\chi_F+2\chi_2^{\perp}\sin^2\theta+2\chi_4^{\perp}\sin^4\theta\right)+\cos\theta\sin(\varphi-\psi)\chi_D\right], \tag{C4}$$

$$\mathcal{T}_\varphi=\frac{\gamma j}{1+\alpha^2}\left[-\cos\theta\sin(\varphi-\psi)\left(\chi_F+\chi_2^{\perp}\sin^2\theta+\chi_4^{\perp}\sin^4\theta\right)+\cos(\varphi-\psi)\left(\chi_D+\chi_2^{\parallel}\sin^2\theta+\chi_4^{\parallel}\sin^4\theta\right)\right]. \tag{C5}$$

No switching. Magnetization reversal is impossible if there exists a value of θ for which the following equation is satisfied:

$$\begin{aligned}&\cos(\varphi-\psi)\left(\chi_F+2\chi_2^{\perp}\sin^2\theta+2\chi_4^{\perp}\sin^4\theta\right)\\ &+\cos\theta\sin(\varphi-\psi)\chi_D=0,\end{aligned} \tag{C6}$$

signifying zero $\mathcal{T}_\theta$ [see Eq. (C4)]. This happens when either of the following cases is realized:

$$\chi_F+2\chi_2^{\perp}+2\chi_4^{\perp}=0, \tag{C7}$$

$$\begin{cases}\chi_D=0,\\ \chi_F+2\chi_2^{\perp}\sin^2\theta+2\chi_4^{\perp}\sin^4\theta=0.\end{cases} \tag{C8}$$

The latter case translates into the conditions on χ_F, $\chi_2^{\perp}$, $\chi_4^{\perp}$ by demanding at least one of the roots of $f(y)\equiv\chi_F+2\chi_2^{\perp}y+2\chi_4^{\perp}y^2$ lie in the range from 0 to 1.

Zero φ torque. The model given by Eq. (3) shows that the optimal ratio of the SOT coefficients corresponds to zero current-induced torque in the direction of increasing φ. While it remains to be seen whether the same result holds for the extended model, it is interesting to see what ratio of the SOT coefficients ensures no current-induced torque in the φ direction – the direction irrelevant for switching.

We start by finding the optimal current angle that provides the largest torque in the θ direction ($\partial\mathcal{T}_\theta/\partial\psi=0$),

$$\psi=\varphi+\arctan\left[\frac{\chi_D\cos\theta}{\chi_F+2\chi_2^{\perp}\sin^2\theta+2\chi_4^{\perp}\sin^4\theta}\right], \tag{C9}$$

and substitute that in Eq. (C5). The expression for the φ component of the SOT becomes

$$\mathcal{T}_\varphi=\frac{\sin^2\theta\left[\chi_D\cos^2\theta\left(\chi_2^{\perp}+\chi_4^{\perp}\sin^2\theta\right)+\left(\chi_D-\chi_2^{\parallel}-\chi_4^{\parallel}\sin^2\theta\right)\left(\chi_F+\chi_2^{\perp}\sin^2\theta+\chi_4^{\perp}\sin^4\theta\right)\right]}{\sqrt{\chi_D^2\cos^2\theta+\left[\chi_F+\chi_2^{\perp}\sin^2\theta+\chi_4^{\perp}\sin^4\theta\right]^2}}. \tag{C10}$$

It follows from Eq. (C10) that the current-induced torque in the φ direction vanishes for all values of θ in any of the four cases:

$$\chi_2^{\perp}=0,\qquad \chi_2^{\parallel}=\chi_D,\quad \chi_4^{\perp}=0,\quad \chi_4^{\parallel}=0, \tag{C11}$$

$$2\chi_2^{\perp}=-\chi_F,\quad 2\chi_2^{\parallel}=\chi_D,\quad \chi_4^{\perp}=0,\quad \chi_4^{\parallel}=0, \tag{C12}$$

$$\chi_D=0,\qquad \chi_2^{\parallel}=0,\quad \chi_4^{\perp}=0,\quad \chi_4^{\parallel}=0, \tag{C13}$$

$$\chi_F=0,\qquad \chi_2^{\perp}=0,\quad \chi_4^{\perp}=0,\quad \chi_4^{\parallel}=0. \tag{C14}$$

However, only Eqs. (C11) and (C13) are relevant as the other two represent special cases of the no-switching condition [see Eq. (C7)].

* These authors contributed equally to this work

† Corresponding author: bessarab@hi.is

[1] P. Gambardella and I. M. Miron, Philos. Trans. R. Soc. A **369**, 3175 (2011).
[2] I. M. Miron, K. Garello, G. Gaudin, P.-J. Zermatten, M. V. Costache, S. Auffret, S. Bandiera, B. Rodmacq, A. Schuhl, and P. Gambardella, Nature **476**, 189 (2011).
[3] L. Liu, C.-F. Pai, Y. Li, H. W. Tseng, D. C. Ralph, and R. A. Buhrman, Science **336**, 555 (2012).
[4] S. V. Aradhya, G. E. Rowlands, J. Oh, D. C. Ralph, and R. A. Buhrman, Nano Lett. **16**, 5987 (2016).
[5] K. Garello, C. O. Avci, I. M. Miron, M. Baumgartner, A. Ghosh, S. Auffret, O. Boulle, G. Gaudin, and P. Gambardella, Appl. Phys. Lett. **105**, 212402 (2014).
[6] K.-S. Lee, S.-W. Lee, B.-C. Min, and K.-J. Lee, Appl. Phys. Lett. **102**, 112410 (2013).
[7] S. Fukami, T. Anekawa, C. Zhang, and H. Ohno, Nat. Nanotechnol. **11**, 621 (2016).
[8] T. Taniguchi, S. Mitani, and M. Hayashi, Phys. Rev. B **92**, 024428 (2015).
[9] J. M. Lee, J. H. Kwon, R. Ramaswamy, J. Yoon, J. Son, X. Qiu, R. Mishra, S. Srivastava, K. Cai, and H. Yang, Commun. Phys. **1**, 2 (2018).
[10] C. O. Avci, K. Garello, C. Nistor, S. Godey, B. Ballesteros, A. Mugarza, A. Barla, M. Valvidares, E. Pellegrin, A. Ghosh, *et al.*, Phys. Rev. B **89**, 214419 (2014).
[11] Y.-C. Lau, D. Betto, K. Rode, J. M. D. Coey, and P. Stamenov, Nat. Nanotechnol. **11**, 758 (2016).
[12] A. van den Brink, G. Vermijs, A. Solignac, J. Koo, J. T. Kohlhepp, H. J. M. Swagten, and B. Koopmans, Nat. Commun. **7**, 10854 (2016).
[13] S. Fukami, C. Zhang, S. DuttaGupta, A. Kurenkov, and H. Ohno, Nat. Mater. **15**, 535 (2016).
[14] Y.-W. Oh, Sh. C. Baek, Y. M. Kim, H. Y. Lee, K.-D. Lee, C.-G. Yang, E.-S. Park, K.-S. Lee, K.-W. Kim, G. Go, *et al.*, Nat. Nanotechnol. **11**, 878 (2016).
[15] G. Yu, P. Upadhyaya, Y. Fan, J. G. Alzate, W. Jiang, K. L. Wong, S. Takei, S. A. Bender, L.-T. Chang, Y. Jiang, *et al.*, Nat. Nanotechnol. **9**, 548 (2014).
[16] G. Yu, P. Upadhyaya, K. L. Wong, W. Jiang, J. G. Alzate, J. Tang, P. K. Amiri, and K. L. Wang, Phys. Rev. B **89**, 104421 (2014).
[17] J. Torrejon, F. Garcia-Sanchez, T. Taniguchi, J. Sinha, S. Mitani, J.-V. Kim, and M. Hayashi, Phys. Rev. B **91**, 214434 (2015).
[18] L. You, O. Lee, D. Bhowmik, D. Labanowski, J. Hong, J. Bokor, and S. Salahuddin, Proc. Natl. Acad. Sci. U.S.A. **112**, 10310 (2015).
[19] L. Liu, C. Zhou, X. Shu, C. Li, T. Zhao, W. Lin, J. Deng, Q. Xie, S. Chen, J. Zhou, *et al.*, Nat. Nanotechnol. **16**, 277 (2021).
[20] Sh. C. Baek, V. P. Amin, Y.-W. Oh, G. Go, S.-J. Lee, G.-H. Lee, K.-J. Kim, M. D. Stiles, B.-G. Park, and K.-J. Lee, Nat. Mater. **17**, 509 (2018).
[21] C. Thirion, W. Wernsdorfer, and D. Mailly, Nat. Mater. **2**, 524 (2003).
[22] Z. Z. Sun and X. R. Wang, Phys. Rev. B **74**, 132401 (2006).
[23] K. Rivkin and J. B. Ketterson, Appl. Phys. Lett. **89**, 252507 (2006).
[24] Z. Z. Sun and X. R. Wang, Phys. Rev. Lett. **97**, 077205 (2006).
[25] G. Woltersdorf and C. H. Back, Phys. Rev. Lett. **99**, 227207 (2007).
[26] G. Bertotti, I. D. Mayergoyz, C. Serpico, M. d'Aquino, and R. Bonin, J. Appl. Phys. **105**, 07B712 (2009).
[27] N. Barros, M. Rassam, H. Jirari, and H. Kachkachi, Phys. Rev. B **83**, 144418 (2011).
[28] N. Barros, H. Rassam, and H. Kachkachi, Phys. Rev. B **88**, 014421 (2013).
[29] L. Cai, D. A. Garanin, and E. M. Chudnovsky, Phys. Rev. B **87**, 024418 (2013).
[30] X. R. Wang, and Z. Z. Sun, Phys. Rev. Lett. **98**, 077201 (2007).
[31] O. A. Tretiakov, Y. Liu, and A. Abanov, Phys. Rev. Lett. **105**, 217203 (2010).
[32] Y. Zhang, H. Y. Yuan, X. S. Wang, and X. R. Wang, Phys. Rev. B **97**, 144416 (2018).
[33] P. M. Haney, H.-W. Lee, K.-J. Lee, A. Manchon, and M. D. Stiles, Phys. Rev. B **87**, 174411 (2013).
[34] J. Yoon, S.-W. Lee, J. H. Kwon, J. M. Lee, J. Son, X. Qiu, K.-J. Lee, and H. Yang, Sci. Adv. **3**, e1603099 (2017).
[35] G. J. Kwiatkowski, M. H. A. Badarneh, D. V. Berkov, and P. F. Bessarab, Phys. Rev. Lett. **126**, 177206 (2021).
[36] `shorturl.at/jvIN2`.
[37] Thermal stability factor is defined as a ratio between the energy barrier and the thermal energy.
[38] As long as $\alpha\xi_D \neq \xi_F$.
[39] G. Go, S.-J. Lee, and K.-J. Lee, Phys. Rev. B **95**, 184401 (2017).
[40] G. Klughertz, P.-A. Hervieux, and G. Manfredi, J. Phys. D: Appl. Phys. **47**, 345004 (2014).
[41] G. Klughertz, L. Friedland, P.-A. Hervieux, and G. Manfredi, Phys. Rev. B **91**, 104433 (2015).
[42] J. Kim, J. Sinha, M. Hayashi, M. Yamanouchi, S. Fukami, T. Suzuki, S. Mitani, and H. Ohno, Nat. Mater. **12**, 240 (2013).
[43] X. Qiu, P. Deorani, K. Narayanapillai, K.-S. Lee, K.-J. Lee, H.-W. Lee, and H. Yang, Sci. Rep. **4**, 4491 (2014).
[44] R. Ramaswamy, X. Qiu, T. Dutta, S. D. Pollard, and H. Yang, Appl. Phys. Lett. **108**, 202406 (2016).
[45] A. Manchon, J. Železný, I. M. Miron, T. Jungwirth, J. Sinova, A. Thiaville, K. Garello, and P. Gambardella, Rev. Mod. Phys. **91**, 035004 (2019).
[46] M. Filianina, J.-P. Hanke, K. Lee, D.-S. Han, S. Jaiswal, A. Rajan, G. Jakob, Y. Mokrousov, and M. Kläui, Phys. Rev. Lett. **124**, 217701 (2020).
[47] S. Ding, A. Ross, D. Go, L. Baldrati, Z. Ren, F. Freimuth, S. Becker, F. Kammerbauer, J. Yang, G. Jakob, Y. Mokrousov, and M. Kläui, Phys. Rev. Lett. **125**, 177201 (2020).
[48] K. Garello, I. M. Miron, C. O. Avci, F. Freimuth, Y. Mokrousov, S. Blügel, S. Auffret, O. Boulle, G. Gaudin, and P. Gambardella, Nat. Nanotechnol. **8**, 587 (2013).
[49] M. Abramowitz and I. A. Stegun, *Handbook of mathematical functions with formulas, graphs, and mathematical tables*, Vol. 55 (US Government printing office, 1948).
[50] J. H. Mentink, M. V. Tretyakov, A. Fasolino, M. I. Katsnelson, and T. Rasing, J. Phys. Condens. Matter **22**, 176001 (2010)
.